


Generation of Electromechanical Frequency Combs in Fluid Media with a Parametrically Driven Capacitive Microresonator

Sushruta Surappa¹, Charles Wei¹, Molei Tao², and F. Levent Degertekin^{1,*}

¹*Woodruff School of Mechanical Engineering, Georgia Institute of Technology, Atlanta, Georgia, USA*

²*Department of Mathematics, Georgia Institute of Technology, Atlanta, Georgia, USA*

 (Received 13 June 2022; revised 21 December 2022; accepted 15 February 2023; published 6 April 2023; corrected 18 July 2023)

The generation of electromechanical frequency combs in both air and liquid environments using a capacitive microresonator array is presented in this paper. In contrast to frequency-comb generation in purely mechanical resonators, we show that the damping-dependent threshold for comb generation can be reduced by parametrically coupling a resonant electrical circuit to the mechanical resonator. A one-dimensional lumped parameter model of the proposed system is presented and semianalytical solutions are developed to investigate the parameters influencing frequency-comb formation under various operating conditions. The results obtained with numerical simulations are experimentally validated using a commercially available microelectromechanical resonator, and frequency combs with a repetition rate sensitive to the force on the mechanical resonator are generated with a single electrical drive in air and in a liquid-filled microfluidic channel. In contrast to prior work on electromechanical frequency combs, this work represents a simple yet robust approach to generating stable combs, thereby enabling its practical use in applications, such as gas sensing and microfluidics.

DOI: [10.1103/PhysRevApplied.19.044021](https://doi.org/10.1103/PhysRevApplied.19.044021)

I. INTRODUCTION

Frequency combs consist of a set of equally spaced, coherent spectral lines that take the form of pulse train in the time domain and resemble the teeth of a comb in the frequency domain. Originally developed as a laser-based tool, optical frequency combs have enabled significant advances in fundamental science and applications, such as absolute distance measurement [1,2], spectroscopy [3], communication [4], frequency metrology [5], and quantum computing [6]. More recently there has been a significant push to realize the mechanical or phononic equivalent of these optical frequency combs [7–10]. The development of a set of stable, broadband mechanical frequency combs would enable the use of comb technology in water and other biologic fluids [11,12], which typically reflect or strongly attenuate light.

The generation of such mechanical frequency combs has been demonstrated in various micro- and nanoscale systems by taking advantage of nonlinear modal interactions at small length scales. When subjected to a strong driving force, the different vibrational modes of a mechanical resonator are coupled to each other via intrinsic nonlinearities leading to the formation of frequency combs. Mechanical frequency combs have been reported using

both single [10,13–15] and multiple drive tones [8,16] and by coupling two or more vibrational modes in a single resonator [17,18]. However, most efforts to date have either been restricted to comb generation in high- Q resonators at low temperatures and pressures or to a narrow frequency band confined within the vibrational mode of the resonator, primarily because the parametric mode coupling that governs comb generation is damping dependent and requires low loss to efficiently enable coupling between the different mechanical modes. Furthermore, great care is required to precisely engineer the device such that the various mechanical modes display a commensurate resonance frequency relationship required for parametric excitation. These characteristics are especially limiting for applications in liquid, where resonators are typically subjected to large mechanical damping. Narrowband frequency-comb generation can also be limiting in metrology applications where a larger bandwidth enables more accurate range measurement [19]. For these reasons, mechanical frequency combs have been used in a limited number of practical applications thus far [20].

In this paper, we present a significantly different approach to mechanical frequency-comb generation wherein a microelectromechanical (MEM) resonator parametrically coupled to a resonant electrical circuit serves as the electromechanical comb generation system. The concept of parametrically coupling a mechanical and electrical

*levent.degertekin@me.gatech.edu

resonator has been previously exploited for wireless power transfer [21] and vibration control [22], where it was found that the initiation threshold for parametric resonance could be lowered by reducing the electrical resistance of the system—thereby overcoming a critical limitation affecting purely mechanical parametrically coupled systems. We adopt this strategy to terminate the MEM resonator with a series inductor and drive it with a single electrical tone to generate evenly spaced, coherent electromechanical frequency combs. The influence of mechanical damping on the input forcing threshold can be minimized by reducing the circuit electrical losses, allowing us to generate frequency combs in lightly (air) and heavily damped (liquid) environments. As the resonance frequency of the electrical oscillator can be controlled by simply adjusting the value of inductance, the proposed approach further enables us to easily obtain the required commensurate frequency relationship between the coupled resonators, independent of the mechanical design and operating conditions.

We start by introducing a one-dimensional (1D) lumped parameter mathematical model to describe the proposed comb generation system, followed by numerical simulations to investigate the influence of model parameters and operating conditions on the formation of frequency combs. Experiments are then performed using a commercial MEM resonator to validate the numerical results and to demonstrate frequency-comb generation in air and in a fluid-filled microfluidic channel. Semianalytical solutions to the 1D model indicate that the input forcing threshold required to generate evenly spaced frequency combs is a function of both the mechanical and electrical damping, and that the threshold can be lowered by reducing the electrical resistance in the circuit. Experimental results further confirm that stable frequency combs can be generated in different media with the same MEM resonator, using a single electrical drive tone. The potential advantage of such comb-based sensor systems over conventional resonant sensors, especially in fluid-sensing applications is also briefly discussed.

II. MATHEMATICAL MODELING

A simplified 1D lumped parameter model of the proposed electromechanical frequency-comb generation system is shown in Fig. 1. The device consists of an electrostatically driven mechanical resonating element that is represented by a parallel-plate baffled piston in this 1D approximation. The piston has an equivalent mass m , stiffness k , and damping b , and is radiating into a fluid half-space. The damping term includes only the radiation losses in the fluid while the structural losses in the resonator are ignored as they are negligible in comparison. The parallel-plate piston, which acts as a time-varying capacitor with static capacitance C_0 in the electrical domain, is connected to an inductor L and resistor R (representing the

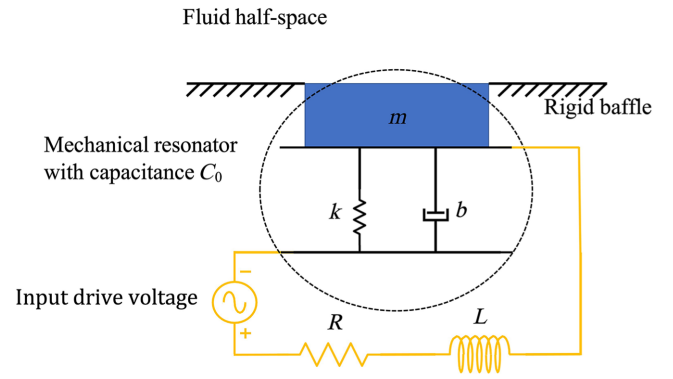


FIG. 1. 1D lumped parameter representation of the electromechanical frequency-comb generation system. The capacitive mechanical resonator is approximated by a baffled parallel-plate piston and electrically terminated in series with an inductor, resistor and a voltage source.

total electrical resistance in the circuit including parasitic resistance) to form a series RLC circuit driven by a voltage source. Note that the mechanical resonance frequency of the parallel-plate piston, mechanical Q factor, electrical resonance frequency of the RLC circuit and electrical Q factor is given by $\omega_m = \sqrt{k/m}$, $Q_m = \omega_m m/b$, $\omega_{el} = 1/\sqrt{LC_0}$, and $Q_e = \omega_{el} L/R$, respectively. Mathematically, the 1D model can be expressed by the following coupled second-order ordinary differential equations (ODEs):

$$\left[\frac{d^2}{dt^2} + \frac{b}{m} \frac{d}{dt} + \frac{k}{m} \right] x = \frac{\epsilon_0 A}{2m} \frac{V_c^2}{(d_0 - x)^2}, \quad (1)$$

$$\left[\frac{d^2}{dt^2} + \frac{R}{L} \frac{d}{dt} + \frac{d_0 - x}{LA\epsilon_0} \right] V_c = \frac{d_0 - x}{LA\epsilon_0} V_{in} \sin(\omega_{in} t), \quad (2)$$

where Eq. (1) represents the dynamics of the mechanical resonator and Eq. (2) represents the electrical resonator. d_0 and x represent the initial gap between the parallel plates of the piston and the displacement of the piston, respectively, whereas V_c , A , and ϵ_0 are the voltage across the variable capacitor, the area of the piston and the permittivity of free space. The term on the right-hand side of Eq. (2) represents the sinusoidal input voltage applied to the circuit having an amplitude V_{in} and frequency ω_{in} [note that in order to obtain Eq. (2), it is assumed that the change in capacitance due to the motion of the plate is much smaller than the static capacitance, i.e., $\Delta C \ll C_0$]. When the system parameters are selected such that the electrical resonance frequency is approximately half the mechanical resonance frequency ($\omega_{el} \approx \omega_m/2$), the two resonators can be parametrically coupled to each other to enable nonlinear modal interactions under certain input excitation conditions. These interactions result in the formation of frequency combs in the electrical as well as in the mechanical domain.

The transient response of the 1D lumped parameter model is analyzed by solving the coupled equations numerically using a commercial solver such as MATLAB. However, this method of solution can be both nonintuitive and time consuming, especially when performing extensive parametric studies. Alternatively, the coupled ODEs can be rewritten using different scaled and normalized parameters to make explicit a timescale separation, and approximated using an improved averaging theory [23,24] to obtain approximate semianalytical solutions (details of the parameters used and the analysis are presented within the Supplemental Material [25]). The semianalytical solutions provide more insight into the operation of the proposed comb generation system by providing expressions for critical drive voltage and frequency-comb spacing. These expressions can be used to explore the dependency of comb generation on a range of environmental and system parameters such as mechanical damping, electrical resistance, and operating frequency. Thus, analysis of the 1D model using a combination of the complete numerical solution and the approximate semianalytical techniques can be used to guide the selection of optimal operating parameters to generate stable frequency combs in different media.

III. RESULTS

A. Mechanical resonator array

A capacitive MEM resonator array is used as a testbed to demonstrate the proposed approach to frequency-comb generation. Such MEM resonator arrays have previously been used for chemical and biological sensing in both fluid and gas environments [26–30]. Here, we use a commercially available (Phillips innovations) MEM array [Fig. 2(a)] consisting of 128 elements, with each element composed of 42 electrostatically actuated membrane-based drumhead resonators connected in parallel. The circular membranes measure $120\ \mu\text{m}$ in diameter and are covered by a thin layer of metal to form a top electrode [Fig. 2(b)]. All 128 elements are separated from a common bottom electrode by a vacuum-filled cavity measuring approximately $450\ \text{nm}$. This vacuum gap corresponds to the full range of mechanical motion of the membranes when they are electrostatically actuated using the top and bottom electrodes. Note that each membrane operates in its fundamental or first mode for the selected frequency range of operation. Furthermore, the operating frequency is selected such that it is far away from the band in which acoustic crosstalk is dominant [31], thereby ensuring that all the membranes in the array oscillate in-phase and higher-order array modes are suppressed. As each individual metalized membrane forms a minicapacitor with the bottom electrode, the MEM array also behaves as a time-varying capacitor and can be terminated with an inductor to realize an inductor-capacitor (LC) electrical resonator.

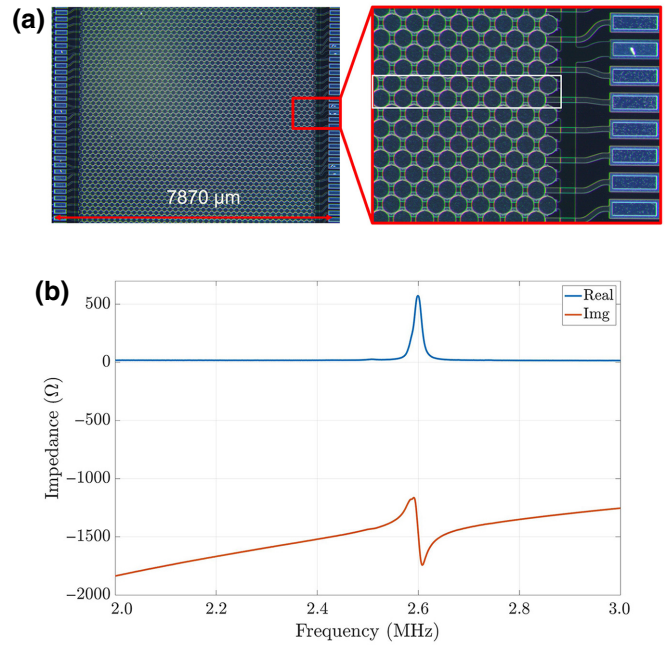


FIG. 2. (a) Top view of the MEM array used in the experiments with the enlarged inset showing the arrangement of the individual membrane resonators. (b) The real and imaginary parts of the impedance measured by connecting two elements in parallel shows a mechanical resonance at 2.6 MHz when biased at 10 VDC.

Two adjacent elements of the MEM array [highlighted by the white box in Fig. 2(a)] are connected in parallel to form the active mechanical resonator for the experiment. The corresponding mechanical and electrical parameters are characterized using a vector network analyzer (Agilent 8753ES) and shown in Fig. 2(b). The mechanical resonance frequency in air is measured to be 2.60 MHz when a 10-V dc bias is applied (note that the unbiased mechanical frequency of the resonator is closer to 2.61 MHz as the application of bias voltage leads to a reduction in resonance frequency due to spring softening [32]). The mechanical Q factor estimated from the bandwidth of the resonance peak is approximately 200, reflecting the low damping experienced by the resonator in air. The static

TABLE I. System parameters used in the numerical simulations.

Parameter	Symbol	Value
Equivalent mass	m (Kg)	1.1155×10^{-8}
Equivalent stiffness	k (N/m)	3×10^6
Equivalent damping	b (N-s/m)	9.1468×10^{-4}
Area of plates	A (m ²)	2.08×10^{-6}
Gap between plates	d_0 (m)	450×10^{-9}
Resistance	R (Ω)	60
Inductance	L (H)	3.6343×10^{-4}
Permittivity	ϵ_0 (F/m)	8.854×10^{-12}

capacitance of the active elements can also be extracted by fitting a curve to the imaginary impedance and is found to be roughly 42 pF. The parameters extracted from the experimental device are used to fully model the electromechanical comb generation system in the numerical simulations and to inform the selection of electrical components in the experiment.

B. Numerical results

The 1D model of the comb generation system described in Sec. II is solved numerically using the parameters listed in Table I with the aim of investigating the influence of various system parameters and operating conditions on the formation of mechanical frequency combs. The input drive frequency and electrical circuit parameters are selected such that $\omega_{\text{in}} = \omega_m/2 = \omega_{\text{el}}$; this 2:1 resonance frequency

relationship is intentionally selected to enable parametric coupling between the mechanical and electrical resonator. Equations (1) and (2) are solved simultaneously using the ODE45 package in MATLAB, and the simulation results obtained are shown in Fig. 3(a). It is observed that for small values of input voltage V_{in} , the solutions for the variables V_c and x , i.e., the voltage across the capacitor and piston displacement, are purely harmonic oscillations at ω_{in} and $2\omega_{\text{in}}$, respectively. However, when V_{in} exceeds a critical input threshold $V_{\text{in crit}}$, a bifurcation appears and equally spaced spectral lines or frequency combs with spacing $\Delta\omega$ are generated on either side of ω_{in} and $2\omega_{\text{in}}$, in both the mechanical and electrical domains. Additionally, the temporal response of the two oscillators takes the form of a pulse train having a beat frequency equal to $\Delta\omega$, which is characteristic of frequency-comb generation systems.

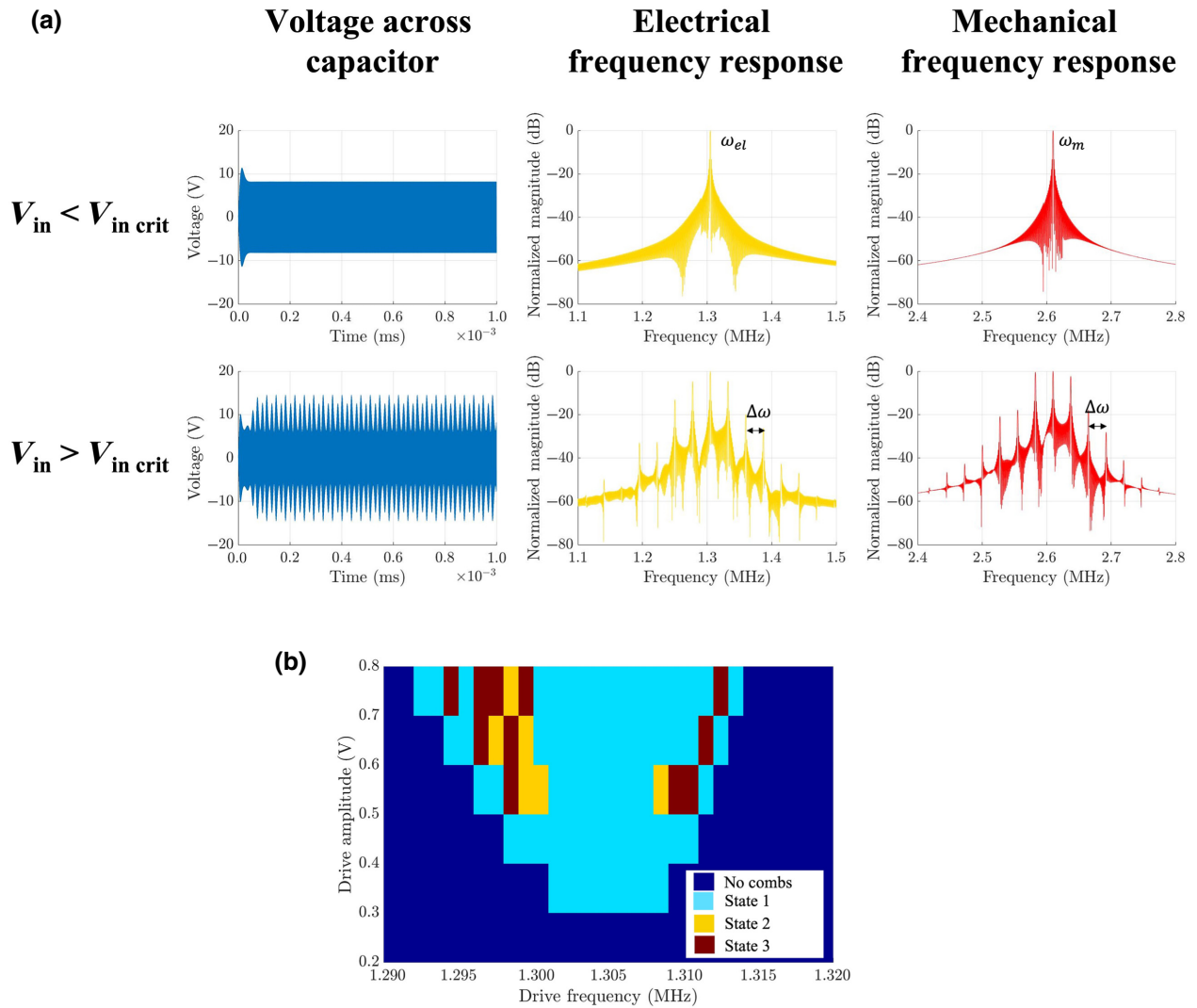


FIG. 3. (a) Simulated response of the 1D frequency-comb generation model when the input voltage is below and above the critical voltage required for comb generation. (b) A 2D colormap representing the locations of frequency-comb formation in the frequency-forcing space. Here, states 1, 2, and 3 represent stable combs, higher-order combs, and chaotic combs, respectively.

The effect of detuning the input drive frequency from the electrical resonance frequency is studied by sweeping $\omega_{\text{in}}/2\pi$ from 1.29 to 1.32 MHz (steps of 1 kHz) at different input drive levels (steps of 0.1 V). The coupled equations are solved for a fixed time of 1 ms with a step size of 25 ns at each discrete frequency and voltage value. It can be seen in Fig. 3(b) that $V_{\text{in crit}}$ increases as ω_{in} is detuned either side of ω_{el} on the frequency axis. The shaded regions where frequency combs are generated are slightly asymmetric about ω_{el} , similar to an instability tongue seen in parametrically excited systems [33]. The types of combs generated within this instability can be classified into three states, where state 1 represents the most commonly occurring stable frequency combs. The squares labeled as state 2 occur at higher levels of forcing and represent regions where higher-order frequency combs are generated, caused by the nonlinear interaction of state-1 combs with each other. Finally state 3 represents frequency combs that demonstrate chaotic behavior. The transient response of the system at these frequencies is highly unstable and frequently resulted in the ODE45 solver crashing. The frequency spectrum of the generated combs in each of these 3 states can be found within the Supplemental Material [25].

The semianalytical solutions developed for Eqs. (1) and (2) can be used to determine the impact of external

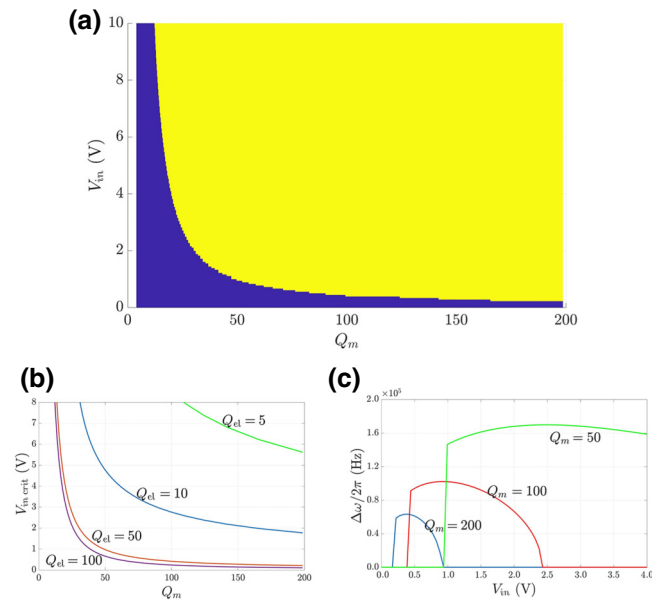


FIG. 4. (a) A 2D plot obtained using the semianalytical solution displaying the dependance of comb generation on input voltage (V_{in}) and mechanical quality factor (Q_m), where the yellow-shaded region represents the existence of frequency combs. (b) Variation of $V_{\text{in crit}}$ as a function of Q_m for decreasing values of Q_{el} . (c) Frequency spacing between comb lines as a function of V_{in} for different Q_m .

operating conditions on frequency-comb generation. The critical threshold value $V_{\text{in crit}}$, can be numerically determined for a given set of system parameters and is found to be dependent on the mechanical damping b , i.e., proportional to the reciprocal of the mechanical Q factor. A map of the regions where frequency combs exist in the $V_{\text{in}} - Q_m$ space when $Q_{\text{el}} = 50$ is shown in Fig. 4(a), with the yellow shaded region indicating the existence of combs. Here, the boundary separating the yellow region from the rest of the map represents $V_{\text{in crit}}$, which increases dramatically with reduced Q_m . While light damping might not impede the ability to generate frequency combs in air, the dependence of $V_{\text{in crit}}$ on b introduces a significant challenge while trying to generate combs using purely mechanical resonators in heavily damped media such as water and biofluids. Fortunately, it is found that in the case of the parametrically coupled electrical-mechanical resonator, $V_{\text{in crit}}$ is a function of both mechanical damping and the resistance R in the electrical circuit. Figure 4(b) shows how the critical input voltage required for parametric resonance reduces with increasing value of electrical quality factor Q_{el} , for a fixed value of Q_m . Hence maintaining a low value of R can partially mitigate the effect of mechanical damping on $V_{\text{in crit}}$ thereby allowing for practically achievable values of $V_{\text{in crit}}$ even at large values of b .

The semianalytical solutions can also be used to predict the spacing between the spectral lines, both as a function of the input drive voltage as well as environmental conditions. The frequency spacing $\Delta\omega$ is plotted against V_{in} for different values of Q_m in Fig. 4(c). While $\Delta\omega$ is initially zero at low values of input drive, a sudden jump or discontinuity in the curve is observed when $V_{\text{in}} = V_{\text{in crit}}$, indicating the onset of frequency-comb generation. The spacing between the comb lines initially increases with increasing V_{in} , before it reaches a maximum value and then gradually begins to decrease. Furthermore, the spacing between the combs also increases as the mechanical Q factor is reduced, indicating that frequency combs spanning a larger bandwidth can be obtained in heavily damped environments. It is worthwhile to note here that the semianalytical solutions are approximate solutions to Eqs. (1) and (2) and as such are not accurate, especially for $V_{\text{in}} \gg V_{\text{in crit}}$. They are better suited to qualitatively inform trends as opposed to quantitative predictions, which require one to fully solve the coupled equations.

Hence the 1D model allows us to investigate the operational characteristics of the proposed electromechanical comb generation system. The semianalytical solutions shed light on how different operating conditions including mechanical and electrical damping affect frequency comb generation and the comb spacing, while suggesting that careful selection of parameters can lower the critical drive voltage required for comb generation. Since the electrical resistance in a circuit can be easily minimized by various active and passive methods, the proposed system

can potentially be utilized for mechanical frequency-comb generation in hitherto inaccessible damped fluid environments.

C. Experimental results

The results of the numerical analysis are experimentally verified by operating the MEM array in different media, starting with air. The MEM array is terminated with wire-wound inductor of suitable inductance such that the electrical resonance frequency of the LC circuit is half the unbiased mechanical frequency, i.e., $\omega_{el} \approx \omega_m/2 = 1.305$ MHz. Note that circuit components with the lowest series resistance are chosen to minimize the total loss in the electrical resonator, such the electrical Q factor is approximately 50. The circuit is then driven by a tone burst (10 ms ON, 2% duty cycle) from a signal generator (Agilent 33250a) through a rf amplifier for 1.295 MHz $\leq (\omega_{in}/2\pi) \leq 1.308$ MHz and the voltage across the MEMS array is recorded. It is found that at low values of V_{in} that frequency spectrum of V_c consists primarily of the $\omega_{in}/2\pi$ component. However, as the level of V_{in} is increased and crosses the critical threshold ($V_{in\text{ crit}} = 0.4$ V), spectral components at $(\omega_{in} \mp n\Delta\omega)/2\pi$ begin to appear on either side of the drive tone where n is an integer representing the number of sidebands. As expected, the time-domain signal takes the form of a pulse train as seen in Fig. 5. It is observed that further increasing V_{in} beyond $V_{in\text{ crit}}$ results in two phenomena. First, the number of sidebands increases as the input voltage is increased. Secondly it is seen that the frequency spacing between the spectral lines increases with V_{in} as predicted by the numerical simulations [Fig. 6(a)]. This increase in spacing is not linear,

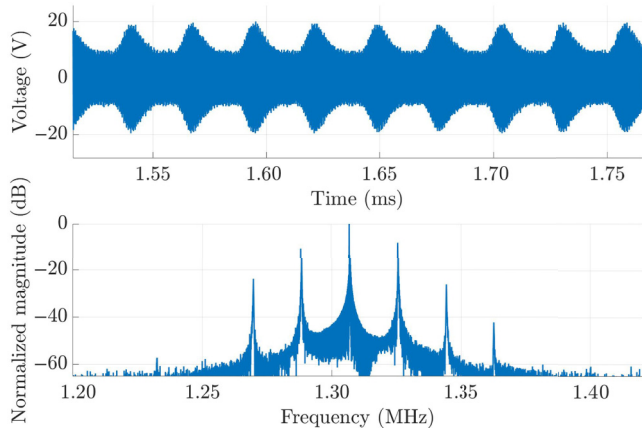


FIG. 5. Voltage measured across the resonator and the corresponding frequency-domain representation of combs when $V_{in} > V_{crit}$ for MEM resonator operating in air. An enlarged view of the time-domain signal demonstrating the interplay between the fundamental oscillation and the nonlinear envelope can be found within the Supplemental Material [25].

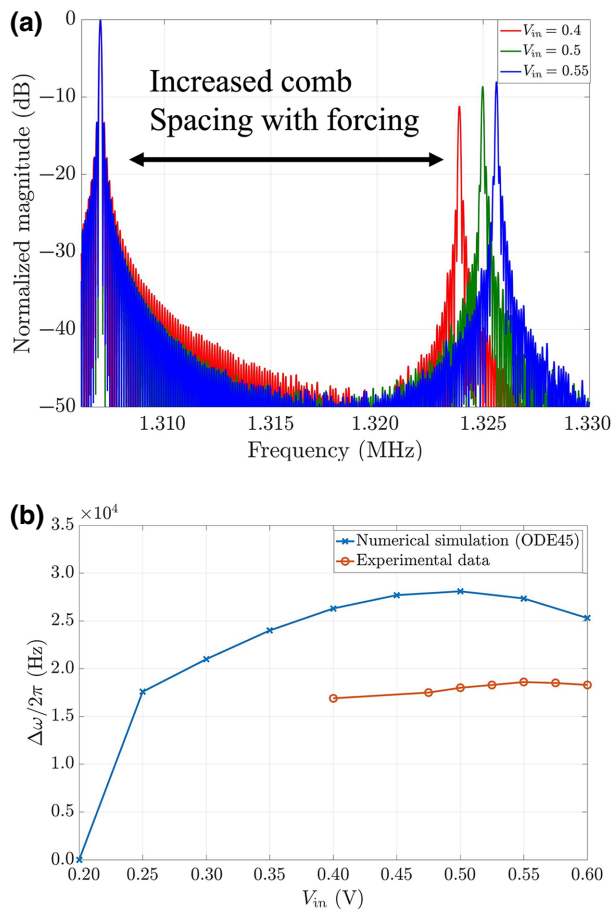


FIG. 6. (a) Increasing spacing between spectral lines observed for larger values of input drive V_{in} . (d) Comparison of the numerical and experimentally obtained change in spectral-line spacing as a function of input voltage V_{in} . Note that no combs are formed below a drive voltage of 0.4 V in the experiment.

with the sharpest change being observed closer to $V_{in\text{ crit}}$, followed by a plateau before eventually reducing at high input voltage levels. Further increasing V_{in} causes nonlinear interactions between the lines, leading to the formation of higher-order combs that results in a highly unstable signal. In order to verify the relation between line spacing and V_{in} , the coupled equations are numerically solved using ODE45 and the results are compared with the experimental data [Fig. 6(b)]. It is found that simulations and experimental data showed a close match, where the offset between the simulated and experimental $\Delta\omega$ can be attributed to nonuniformities in fabrication and parasitic capacitance in the experimental device. Thus, a single drive tone with $V_{in} > V_{in\text{ crit}}$ is sufficient to generate stable frequency combs in the proposed system under lightly damped conditions. The spacing between the spectral lines is directly dependent on V_{in} , which essentially acts as an electrostatic force on the mechanical resonator. Hence, by operating the system at a fixed V_{in} , the change in line

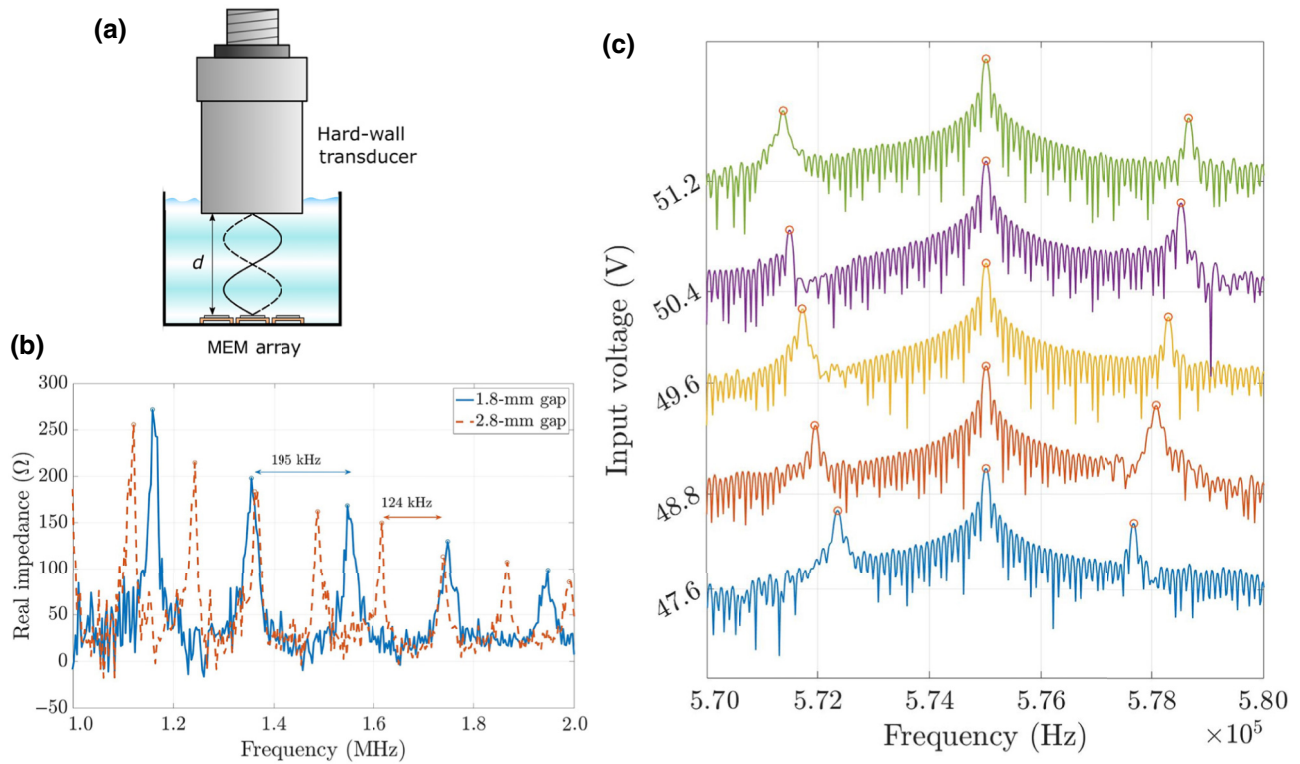


FIG. 7. (a) Experimental setup to simulate boundary conditions of an enclosed microfluidic channel. (b) The effect of channel height d , on the location and spacing between standing-wave resonances. (c) Electromechanical comb spectrum for increasing input voltage levels when the MEM resonator is operated inside a liquid-filled channel.

spacing can be used to directly determine an increment in force or mass acting on the mechanical resonator. Unlike conventional force sensing resonators that require complex electronic feedback loops to track changes in frequency, the proposed system can be monitored by simply tracking the beat frequency using a frequency counter [20].

The same MEM array is next immersed in nonconductive waterlike liquid (Fluorinert-FC 70, Sigma Aldrich) to study the effect of increased mechanical damping on the generation of frequency combs. The frequency response of the mechanical resonator in immersion is first characterized by applying a 50-ns unipolar pulse from a signal generator to the array. The impulse response of the resonator is recorded using a broadband hydrophone (Onda) and from the FFT of the signal (see Supplemental Material [25]), it is seen that the 3-dB bandwidth is 3.15 MHz and the mechanical Q factor is less than 1 when operating in immersion. The additional mass loading and increased damping experienced by the resonator, in contrast to operation in air, leads to a reduction in the mechanical resonance frequency to approximately 1.7 MHz, so the value of the series inductor is adjusted such that the electrical resonance frequency is 850 kHz ($\omega_{el} \approx \omega_m/2$). The system is first driven by a single electrical drive tone at $\omega_{in}/2\pi = 850$ kHz and the spectrum of the signal received by the hydrophone is monitored for increasing drive amplitude

levels. It is observed that for all input drive levels, the output spectrum consists purely of the ω_{in}/π component and no additional spectral lines are observed. This can be explained by the fact that when the resonator operates in immersion, the increased damping causes $V_{in\ crit}$ to exceed the maximum operating voltage of the resonator—as a result, frequency combs are not generated when the resonator is driven by a single drive tone in an open liquid domain.

Alternatively, the case of a resonator operating in a fluid with a rigid boundary is considered, as many biosensing applications consist of an enclosed microfluidic channel through which a fluid of interest is flown and the sensing element is placed inline along the channel. To simulate similar boundary conditions, a MEM array is fixed to the bottom of a container filled with FC-70 and a piezoelectric transducer is placed above at a distance d , with its flat face parallel to the array surface [Fig. 7(a)]. The face of the transducer acts as a hard wall or reflector mimicking the walls of a microfluidic channel and enables the formation of acoustic standing waves between the MEM array and the piezo transducer. These high- Q factor standing-wave resonances can be exploited as the primary vibrational mode of the mechanical resonator to generate frequency combs with a single drive tone in liquid. As the vertical distance d can be adjusted by a screw gauge micrometer,

the position and frequency spacing between the standing waves can be manually tuned to a desired value as seen in Fig. 7(b). The screw gauge is adjusted to obtain a spacing of $d = 1.8$ mm and a standing-wave resonance ($Q_m \approx 13$) is generated at 1.15 MHz ($c_{FC-70} = 687$ m/s). The electrical circuit is tuned to half of this frequency ($\omega_{el} = 575$ kHz) and the system is driven with a single tone at $\omega_{in} = \omega_{el}$. Similar to the behavior in air, it is observed in Fig. 7(c), that additional evenly spaced spectral lines begin to appear on either side of ω_{el} as the input drive is increased above $V_{in\ crit} = 46$ V. The spacing between the spectral lines also increases with higher input voltage levels, confirming the dependency of line spacing on the force experienced by the mechanical resonator. Despite the larger damping experienced in immersion, the confinement of energy within a high- Q standing-wave mode enables the generation of electromechanical frequency combs using a single drive tone, in an enclosed fluid-filled channel. The change in spectral line spacing with increasing forcing further indicates that the generated combs can be used to sense fluid properties or mass of particles in solution in a simple manner without fabrication of complex resonator arrays [34].

To highlight the advantage of comb-based sensing over conventional resonance spectroscopy [35] when interrogating bulk fluid properties in microfluidics, we simulate and compare the frequency response of a linear resonator to a frequency-comb generating resonator, when operating in a 200- μm -high, fluid-filled channel. The methods of solution described in the earlier sections cannot be used to solve this particular problem due to the nontrivial boundary conditions—instead we employ a previously used technique that makes use of SIMULINK [36] (details in Supplemental Material [25]). The sensitivity of the resonator to a 5% change in fluid density is evaluated when operating in these two distinct modes, and the results are

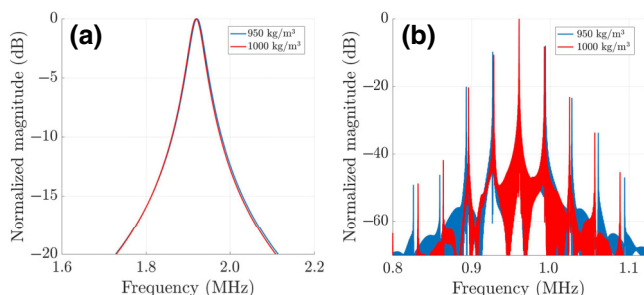


FIG. 8. Numerical simulation comparing the linear frequency response (left) of an electromechanical resonator in a fluid channel to its frequency-comb response when the density of the fluid is reduced by 5%. The change in the frequency spacing between the combs can be seen more clearly as we measure further away from the central spectral line.

shown in Fig. 8. It is observed that in the linear case, the density change produces a negligible shift in both the amplitude and frequency the resonant peak, partly as the low- Q frequency response makes it challenging to accurately detect the peak shift. The time of flight or spacing between the standing-wave resonances cannot be used either as the speed of sound of the medium is held constant. However, a clear and distinguishable separation between the spectral lines for the two different fluid densities can be observed when the resonator is configured to generate frequency combs (the recording length or gate time here is 5 ms). Inherently, the system acts as an amplitude to frequency converter, where the change in operating point on the linear frequency response curve is expressed as a shift in the spectral-line spacing. Furthermore, the frequency shift $\Delta\omega$ is multiplied by a factor n (where n represents the number of spectral lines formed on either side of the driving frequency) as we move away from the central spectral line, resulting in improved sensitivity with a greater number of frequency combs. For example, a frequency spacing of 3 kHz can be observed at the second spectral line from the center, whereas a spacing of 6 kHz is observed at the fourth spectral line, for the same change in density.

It is useful to point out that the spectral-line width can be further reduced by increasing the gate width or acquisition time. The collection of a larger number of data points in the time domain improves the resolution of the combs in the frequency domain, thus enabling higher sensor resolution at the cost of a longer acquisition time. The sensitivity of the comb-based system can also be improved by generating a larger number of equidistant spectral lines on either side of the drive tone, as shown in the simulation. Increasing the strength of the drive tone increases the SNR of the sidebands, however, there is an upper limit on the drive strength beyond which the generated combs become unstable. Alternatively, tuning the bandwidth of the input excitation signal or modifying the nonlinearity that mediates frequency mixing could potentially enable broadband spectral lines as seen in OFCs. Thus, the potential of mechanical comb-based techniques for fluidic measurements and spectroscopy is demonstrated. Further improvements in resolution and sensitivity can be made possible by optimizing the driving voltage and other system parameters, with the ultimate system resolution eventually limited by effects such as thermal fluctuations, external mechanical vibrations, and phase noise.

IV. CONCLUSIONS

In conclusion, we demonstrate the generation of stable electromechanical frequency combs in air and liquid by using a MEM array parametrically coupled to an electrical resonator. A 1D lumped parameter model of the

proposed system is presented, and approximate semianalytical solutions are developed, that allow the investigation of system parameters influencing frequency-comb generation. Numerical simulations reveal that the critical input voltage required to generate frequency combs is a function of both the mechanical Q factor and electrical Q factor. In contrast to purely mechanical resonator-based frequency comb generation methods, the initiation threshold in the proposed system can be lowered by reducing the electrical resistance using passive or active methods, thereby enabling frequency-comb formation even in highly damped environments. The results obtained by numerical simulations are experimentally validated using a commercially available MEM resonator terminated with a wirewound inductor. Frequency combs with a repetition rate sensitive to the force on the mechanical resonator are generated with a single electrical input drive in air and in an enclosed fluid-filled microfluidic channel. The advantage of our approach in sensing applications is highlighted by comparing the performance of a comb-based sensor with conventional resonance spectroscopy when interrogating bulk fluid properties. Thus, the ability to generate stable and tunable electromechanical combs in fluids enables several applications previously inaccessible to optical combs. Future work will be focused on optimizing the proposed system for applications in microfluidic particle detection. The generation of frequency combs in an open fluid domain using a single drive tone will also be explored.

ACKNOWLEDGMENTS

This work is supported by the ECCS division of the National Science Foundation through NSF ECCS Award No. 1936776. Device fabrication is performed in part at the Georgia Tech Institute for Electronics and Nanotechnology, a member of the National Nanotechnology Coordinated Infrastructure (NNCI), which is supported by the National Science Foundation (Grant No. ECCS-2025462). M.T. is grateful for partial support from NSF Grant No. DMS-1847802.

[1] I. Coddington, W. C. Swann, L. Nenadovic, and N. R. Newbury, Rapid and precise absolute distance measurements at long range, *Nat. Photonics* **3**, 351 (2009).
 [2] M.-G. Suh and K. J. Vahala, Soliton microcomb range measurement, *Science* **359**, 884 (2018).
 [3] N. Picqué and T. W. Hänsch, Frequency comb spectroscopy, *Nat. Photonics* **13**, 146 (2019).
 [4] J. Pfeifle, V. Brasch, M. Lauerer, Y. Yu, D. Wegner, T. Herr, K. Hartinger, P. Schindler, J. Li, and D. Hillerkuss, Coherent terabit communications with microresonator Kerr frequency combs, *Nat. Photonics* **8**, 375 (2014).
 [5] T. Udem, R. Holzwarth, and T. W. Hänsch, Optical frequency metrology, *Nature* **416**, 233 (2002).

[6] N. C. Menicucci, S. T. Flammia, and O. Pfister, One-Way Quantum Computing in the Optical Frequency Comb, *Phys. Rev. Lett.* **101**, 130501 (2008).
 [7] I. S. Maksymov, B. Q. Huy Nguyen, A. Pototsky, and S. Suslov, Acoustic, phononic, Brillouin light scattering and Faraday wave-based frequency combs: physical foundations and applications, *Sensors* **22**, 10 (2022).
 [8] I. Mahboob, Q. Wilmart, K. Nishiguchi, A. Fujiwara, and H. Yamaguchi, Tuneable electromechanical comb generation, *Appl. Phys. Lett.* **100**, 113109 (2012).
 [9] L. S. Cao, D. X. Qi, R. W. Peng, M. Wang, and P. Schmelcher, Phononic Frequency Combs through Nonlinear Resonances, *Phys. Rev. Lett.* **112**, 075505 (2014).
 [10] A. Ganesan, C. Do, and A. Seshia, Phononic Frequency Comb via Intrinsic Three-Wave Mixing, *Phys. Rev. Lett.* **118**, 033903 (2017).
 [11] B. Q. H. Nguyen, I. S. Maksymov, and S. A. Suslov, Acoustic frequency combs using gas bubble cluster oscillations in liquids: A proof of concept, *Sci. Rep.* **11**, 1 (2020).
 [12] B. Q. H. Nguyen, I. S. Maksymov, and S. A. Suslov, Spectrally wide acoustic frequency combs generated using oscillations of polydisperse gas bubble clusters in liquids, *Phys. Rev. E* **104**, 035104 (2021).
 [13] D. A. Czaplowski, C. Chen, D. Lopez, O. Shoshani, A. M. Eriksson, S. Strachan, and S. W. Shaw, Bifurcation Generated Mechanical Frequency Comb, *Phys. Rev. Lett.* **121**, 244302 (2018).
 [14] M. Goryachev, S. Galliou, and M. E. Tobar, Generation of ultralow power phononic combs, *Phys. Rev. Res.* **2**, 023035 (2020).
 [15] R. L. Kubena, W. S. Wall, J. Koehl, and R. J. Joyce, Phononic comb generation in high-Q quartz resonators, *Appl. Phys. Lett.* **116**, 053501 (2020).
 [16] A. Ganesan, C. Do, and A. Seshia, Frequency transitions in phononic four-wave mixing, *Appl. Phys. Lett.* **111**, 064101 (2017).
 [17] A. Ganesan, C. Do, and A. Seshia, Phononic frequency comb via three-mode parametric resonance, *Appl. Phys. Lett.* **112**, 021906 (2018).
 [18] M. Park and A. Ansari, Formation, evolution, and tuning of frequency combs in microelectromechanical resonators, *J. Microelectromech. Syst.* **28**, 429 (2019).
 [19] H. Wu, Z. Qian, H. Zhang, X. Xu, B. Xue, and J. Zhai, Precise underwater distance measurement by dual acoustic frequency combs, *Ann. Phys. (Berlin, Ger.)* **531**, 1900283 (2019).
 [20] A. Ganesan and A. Seshia, Resonance tracking in a micromechanical device using phononic frequency combs, *Sci. Rep.* **9**, 1 (2019).
 [21] S. Surappa and F. L. Degertekin, Characterization of a parametric resonance based capacitive ultrasonic transducer in air for acoustic power transfer and sensing, *Sens. Actuators, A* **303**, 111863 (2020).
 [22] S. Surappa and F. L. Degertekin, Passive vibration control and tunable damping of MEMS resonators via electrical autparametric resonance, *J. Microelectromech. Syst.* **30**, 843 (2021).
 [23] J. A. Sanders, F. Verhulst, and J. Murdock, *Averaging Methods in Nonlinear Dynamical Systems* (Springer New York, NY, 2007), Vol. 59.

- [24] M. Tao, Simply improved averaging for coupled oscillators and weakly nonlinear waves, *Commun. Nonlinear Sci. Numer. Simul.* **71**, 1 (2019).
- [25] See Supplementary Material at <http://link.aps.org/supplemental/10.1103/PhysRevApplied.19.044021> for details of semianalytical solutions, comb spectra, resonator frequency response, and SIMULINK model of an enclosed channel.
- [26] M. Thränhardt, P.-C. Eccardt, H. Mooshofer, P. Hauptmann, and L. Degertekin, in *SENSORS, 2009 IEEE* (IEEE, 2009), pp. 878–883.
- [27] M. J. G. Mølgaard, M. Laustsen, M. H. Jakobsen, T. L. Andresen, and E. V. Thomsen, Combined colorimetric and gravimetric CMUT sensor for detection of benzyl methyl ketone, *Sens. Actuators, B* **275**, 483 (2018).
- [28] D. Pelenis, D. Barauskas, G. Vanagas, M. Dzikaras, and D. Viržonis, CMUT-based biosensor with convolutional neural network signal processing, *Ultrasonics* **99**, 105956 (2019).
- [29] K. K. Park, H. Lee, M. Kupnik, Ö Oralkan, J.-P. Ramseyer, H. P. Lang, M. Hegner, C. Gerber, and B. T. Khuri-Yakub, Capacitive micromachined ultrasonic transducer (CMUT) as a chemical sensor for DMMP detection, *Sens. Actuators, B* **160**, 1120 (2011).
- [30] S. Park, I. Yoon, S. Lee, H. Kim, J.-W. Seo, Y. Chung, A. Unger, M. Kupnik, and H. J. Lee, CMUT-based resonant gas sensor array for VOC detection with low operating voltage, *Sens. Actuators, B* **273**, 1556 (2018).
- [31] M. Hochman, PhD Thesis, Georgia Institute of Technology, 2011.
- [32] G. G. Yaralioglu, A. S. Ergun, B. Bayram, E. Haeggstrom, and B. T. Khuri-Yakub, Calculation and measurement of electromechanical coupling coefficient of capacitive micro-machined ultrasonic transducers, *IEEE Trans. Ultrason. Ferroelectr. Freq. Control* **50**, 449 (2003).
- [33] A. H. Nayfeh and D. T. Mook, *Nonlinear Oscillations* (Wiley and sons, Hoboken, NJ, 2008).
- [34] T. P. Burg, M. Godin, S. M. Knudsen, W. Shen, G. Carlson, J. S. Foster, K. Babcock, and S. R. Manalis, Weighing of biomolecules, single cells and single nanoparticles in fluid, *Nature* **446**, 1066 (2007).
- [35] M. Agrawal and A. A. Seshia, in *2016 IEEE International Frequency Control Symposium (IFCS)* (2016), pp. 1–5.
- [36] S. Surappa, M. Tao, and F. L. Degertekin, Analysis and design of capacitive parametric ultrasonic transducers for efficient ultrasonic power transfer based on a 1-D lumped model, *IEEE Trans. Ultrason. Ferroelectr. Freq. Control* **65**, 2103 (2018).
- [37] L. E. Kinsler, A. R. Frey, A. B. Coppens, and J. V. Sanders, *Fundamentals of Acoustics*, 4th ed. (Wiley and sons, Hoboken, NJ, 1999).

Correction: The omission of additional support information has been fixed and added in the last sentence.